Spectroscopic study of precipitates formed during removal of selenium from mine drainage spiked with selenate using permeable reactive materials

KEIKO SASAKI,[1]* DAVID W. BLOWES[2] and CAROL J. PTACEK[2]

[1]Department of Earth Resources Engineering, Faculty of Engineering, Kyushu University, Fukuoka 819-0395, Japan
[2]Department of Earth Sciences, University of Waterloo, ON, N2L 3G1, Canada

The potential for Se removal from mine drainage water using permeable reactive materials was evaluated by a laboratory column experiment. The column materials, organic carbon and zero valence iron (ZVI), were exposed to mine drainage containing 630 mg L^{-1} SO_4^{2-}. The influent water was spiked with 40 mg L^{-1} Se(VI) to assess the potential for Se removal. This high Se(VI) concentration was selected to ensure that there would be a sufficient mass of Se-bearing reaction products available for mineralogical characterization. The experiment was conducted in an anaerobic chamber to replicate the anaerobic conditions that prevail in permeable reactive barrier systems. After loading 10.8 pore volumes of input solution, the column effluent contained <0.002 mg L^{-1} Se and <300 mg L^{-1} SO_4^{2-}. After the column experiments was complete the reactive materials were sampled in the anaerobic chamber and examined using scanning electron microscopy (SEM) coupled with energy dispersion X-ray analysis (SEM-EDAX), X-ray photoelectron spectroscopy (XPS) and by Raman spectroscopy. Sulfate was reduced to sulfide and elemental sulfur, which accumulated on the surfaces of the column materials. Se-bearing precipitates were observed at the base of column. Scanning electron microscopy (SEM) showed the presence of elemental Se, suggesting that Se(VI) was partly reduced to metallic Se(0). The XPS results revealed that selenate was reduced mainly to iron selenide (FeSe and/or $FeSe_2$) on the surface of the column substances. These observations suggest that both chemical reduction and biologically mediated reduction of Se(VI) occurred.

Keywords: selenium, X-ray photoelectron spectroscopy, zero valence iron, permeable reactive barrier, anaerobic condition

INTRODUCTION

Groundwater contamination by Se originates from mine sites, industrial sites and in agricultural drainage (Frankenberg and Benson, 1994). Selenium-bearing minerals are rare, but can be abundant at individual mine sites. Furthermore, Se can substitute for S in sulfide minerals, and therefore Se occurs as an impurity in some sulfide ores. Selenium is an essential element for many species including humans. However, there is a narrow range of Se intake that is beneficial to health. Outside of this range, deficiency diseases and toxicity occur (Fishbein, 1991). As a consequence, regulatory agencies have established water quality guidelines and limits for Se in groundwater.

Permeable reactive barriers (PRB) provide an alternative to conventional pump and treat systems for remediation of contaminated groundwater. PRB systems for the removal of heavy metals, radionuclides, nitrate, phosphate, and arsenic have been utilized at industrial sites and mine sites (Scherer *et al.*, 2000; Blowes *et al.*, 2000). Groundwater contamination by selenate (Se(VI)) potentially is amenable to treatment using a PRB.

Understanding the chemical speciation of the Se retained in the reactive materials is important because Se solubility, bioavailability, and toxicity are strongly influenced by speciation (Presser and Swan, 1990). Selenate (Se(VI)) and selenite (Se(IV)) are more mobile and toxic than elemental selenium (Se(0)) and selenide (Se(-II)). Myneni *et al.* (1997) observed that Se(VI) was reduced to Se(0) by green rust through an abiotic transformation in the presence of Fe(II, III) oxides. The Se speciation of the reaction products was examined using X-ray absorption near edge structure (XANES) and extended X-ray absorption fine structure (EXAFS) spectroscopy studies conducted on aqueous and solid-phase samples. Zhang *et al.* (2005) reported Se(VI) was reduced to Se(IV) and adsorbed onto iron oxyhydroxides formed during the corrosion of zero valence iron (ZVI) under the aerobic conditions, and that the efficiency of Se removal was not significantly inhibited by other anions except for phosphate. Stolz and Oremland (1999) reported that most selenium-reducing bacteria reduce Se(VI) and Se(IV) to Se(0), and not to Se(-II).

*Corresponding author (e-mail: keikos@mine.kyushu-u.ac.jp)

Table 1. Water chemistry of the mine drainage (mg L^{-1})

Al	As	B	Ba	Ca	Cd	Co	Cr	Cu	Fe	K	Li	Mg	Mn	Mo
<0.37	<0.002	0.029	0.049	236	<0.005	<0.009	<0.004	0.01	<0.03	1.82	<0.004	69.2	<0.001	0.029

Na	Ni	P	Pb	S	Se	Si	Sn	Sr	Ti	Tl	V	Zn	pH
<0.014	<0.014	<0.16	<0.068	211	2.24	9.16	<0.055	0.529	0.007	<0.074	0.015	0.019	7.57

The rates of chemical and microbiological reduction are key factors that govern the performance of PRB systems. Microbiological reduction can be sustained through bacterial growth and multiplication, which is maintained by an adequate supply of suitable electron donors for example CH_2, H_2 etc. Chemical reduction requires an adequate supply of a reactive reductant.

The potential for Se(VI) removal using permeable reactive materials was examined through a laboratory scale column experiment in the present study. To understand the process resulting in Se removal, column materials were characterized following the treatment of Se-containing mine drainage using several spectroscopic techniques.

Fig. 1. Assembly of the PRB column experiment.

EXPERIMENTAL

Background water chemistry

The column experiment methodology is described in detail by Sasaki *et al*. (in press). Solids collected at the termination of the experiment were characterized in this study. A brief description of the experiment is provided here. The mine-drainage water for the column influent solution was collected from a mine site near Soda Springs, Idaho. The ore at this site is overlain by the Se-bearing Phosphoria Formation. Oxidation of Se-bearing minerals contained in the overburden results in the release of Se to the groundwater flow system. The groundwater composition is provided in Table 1. The input solution Se concentration was increased to 40 mg L^{-1} as Se, by adding Na_2SeO_4 to the site groundwater. Use of water containing this higher Se concentration facilitated the determination of Se removal mechanisms and rates of Se removal. This increased Se concentration provided the opportunity to detect the chemical speciation of Se after loading Se-impacted water over a limited period. Water derived from the mine site was used to determine whether potentially competing constituents interact with reactive materials to form precipitates and thereby alter the reactivity or permeability of the barrier materials. As previously reported (Sasaki *et al*., in press), the geochemical calculations indicated that the solution was supersaturated with Se (hexagonal, amorphous), FeSe, and $FeSe_2$ (ferroselite).

Column experiments
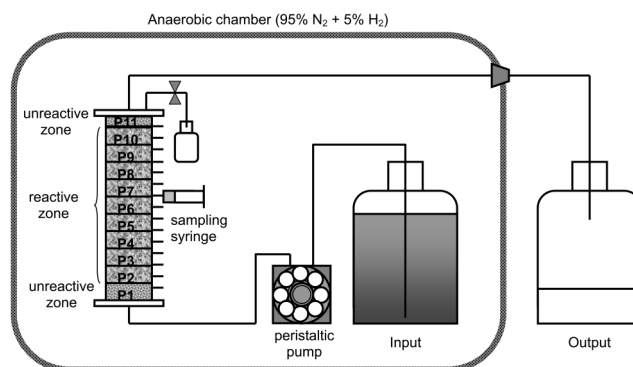
The column was 40 cm in length with an inner diameter of 7.5 cm. The internal volume of the column was 1700 mL. The pore volume of the reactive materials was 662 mL. The calculated porosity of the column was 0.39. The reactive zone in the column (34 cm in length), was filled with reactive material; thin zones at the top (1.8 cm) and bottom (4 cm) were packed with 100% silica sand to isolate the reactive material from the column endplates. The reactive material contained 10 (v/v) % ZVI (ETI-CC-1004; Connelly-GPM, Inc, Chicago), 30(v/v) % silica sand, 20(v/v) % gravel, and 40(v/v) of organic carbon. The organic carbon consisted of 50(v/v) % composted leaf mulch, 25 (v/v) % wood chips, and 25 (v/v) % sawdust. In the column, the reactive material contained 29.06 g ZVI. The ZVI ranged in grain size from less than U.S. Standard Mesh 8 (2.38 mm in grain diameter) to a medium to coarse sand. A small amount of organic stream sediment was added to the reactive mixture. This sediment was taken from an anoxic zone of a small stream that flows through the University of Waterloo. The sediment was not exposed to air prior to being loaded in the column. The sediment was blackish and had a rotten egg-smell. The stream sediment was added to provide an active bacterial consortium which included sulfate reducing bacteria. The presence and the enumeration of sulfate-reducing bacteria in the sediment using the most probable number (MPN) method have been reported to be at least 10^5 cells/g elsewhere (Sasaki *et al*., in press).

Prior to loading the site water, the column was flushed

Table 2. *Electron binding energy (E_B) for some related substances*

Substances	Fe $2p_{3/2}$	Fe $3p_{3/2}$	Se $3p_{3/2}$	Se $3d_{5/2}$	Se $L_3M_{45}M_{45}$	S $2p_{3/2}$	References
Se	—	—	161.7	55.5	—	—	Canava et al. (2002)
	—	—	—	55.2	—	—	Cahen et al. (1985)
	—	—	—	54.7	—	—	Iwakuro et al. (1982)
	—	—	161.6	55.3	180.6	—	the present work
ZnSe	—	—	—	54.1	—	—	Canava et al. (2002)
	—	—	—	54.2	180.6	—	Islam and Rao (1996)
	—	—	161.0	54.9	180.9	—	the present work
GaSe	—	—	—	54.4	180.2	—	Iwakuro et al. (1982)
FeSe	712.0	—	—	53.7	—	—	Hamdadou et al. (2002)
CdSe	—	—	—	53.9	—	—	Canava et al. (2002)
	—	—	—	54.2	—	—	Islam and Rao (1996)
In_2Se_3	—	—	—	53.6	—	—	Canava et al. (2002)
As_2Se_3	—	—	161.0	—	—	—	Ueno and Odajima (1982)
H_2SeO_3	—	—	163.9	59.0	—	—	Bahl et al. (1979)
SeO_2	—	—	165.1	58.8	—	—	Bahl et al. (1979)
H_2SeO_4	—	—	164.4	61.0	—	—	Bahl et al. (1979)
Fe	706.8	—	—	—	—	—	Konno and Nagayama (1980)
Fe[*1]	706.9	52.4	—	—	—	—	the present work
FeS_2	707.0	—	—	—	—	162.2	Sasaki et al. (1993)
S	—	—	—	—	—	164.3	Wagner et al. (1990)
α-Fe_2O_3	711.0	—	—	—	—	—	Konno and Nagayama (1980)
$FeSO_47H_2O$	711.1	—	—	—	—	168.8	Konno et al. (1991)
γ-FeOOH	711.3	—	—	—	—	—	Konno and Nagayama (1980)
Na_2SO_3	—	—	—	—	—	166.6	Wagner et al. (1990)
$Na_2S_2O_3$ central S	—	—	—	—	—	162.5	Wagner et al. (1990)
$Na_2S_2O_3$ peripheral S	—	—	—	—	—	168.6	Wagner et al. (1990)
Untreated ZVI[*2]	712.1[*3]	55.6	—	—	—	—	the present work
Cleaned ZVI[*2]	710.4	55.5	—	—	—	—	the present work

[*1]*Iron foil 99.99% (ALFA) after sputtering for 20 min.*
[*2]*Zero valence iron (ZVI) is supplied by Connelly-GPM, Ins. (Chicago, IL).*
[*3]*Very broad.*

with CO_2 gas for 6 hours to displace less soluble air. The column was then saturated with a 1000 mg L^{-1} (as sulfate) $CaSO_4$ solution containing 5% Na-lactate. The $CaSO_4$/Na-lactate solution was retained in the column for 48 hours to serve as the electron donor to establish sulfate reduction in the column.

The column experiment was conducted in a flexible vinyl anaerobic chamber (Coy Laboratory Products Inc., USA) filled with 7% H_2 and 93% N_2. After the column was sealed inside the anaerobic chamber, the influent water was pumped from an input container to the column by a high-precision peristaltic pump in the anaerobic chamber, as shown in Fig. 1. Flow through the column was upward. The average flow rate was 0.144 L d^{-1}, corresponding to 0.217 pv d^{-1}. This flow rate corresponds to an average linear groundwater velocity of 3.26 cm d^{-1} in the column, and to the residence time of 4.77 d. A total of 7.2 L Se-spiked water was pumped through the column over a period of 1200 h. After the flow was terminated, the column material in a reactive zone was divided into nine vertical sections (3.8 cm thick) corresponding to the sampling-port locations. These samples were labeled P2~P10 in order from the bottom to the top (Fig. 1). As a primary reactive material, ZVI was hand picked and allowed to dry in the anaerobic chamber overnight, prior to the spectroscopic study.

X-ray photoelectron spectroscopy

X-ray photoelectron spectra were collected for ZVI granules from each sample over the binding energy range from 0 to 1200 eV using a VG scientific ESCALab 250 operating in the Al Kα (hν = 1486.6 eV) X-ray radiation mode with the neutralization gun to avoid the differential charging effect, under the following conditions for regional scan: pass energy 20 eV, step energy 0.1 eV, dwell time (time/step) 100 ms, the number of scan 3–20 depending upon the XPS features. The pressures in the analysis and preparation chambers were 10^{-9} and 10^{-5} Torr, respectively. The powders were fixed on conductive carbon tape.

The spectral sets acquired were viewed and processed using the Casa XPS software (Ver. 2.3.12). Background

Table 3. Binding energy (E_B) and full width at half maximum (FWHM) for surface products on column materials after water treatment for 1200 hours

Sample		Fe 2p$_{3/2}$ (1)	Fe 2p$_{3/2}$ (2)	Fe 2p$_{3/2}$ (3)	Fe 3p$_{3/2}$ (1)	Fe 3p$_{3/2}$ (2)	Fe 3p$_{3/2}$ (3)	Se 3d$_{5/2}$	Se L$_3$M$_{45}$M$_{45}$	Se 3p$_{3/2}$	S 2p$_{3/2}$ (1)	S 2p$_{3/2}$ (2)	S 2p$_{3/2}$ (3)	N 1s
P2	E_B/eV	706.8	709.5	714.1	52.8	54.7	56.0	53.3	178.6	160.2	162.0	—	—	399.7
	FWHM	0.9	3.7	8.7	0.7	2.2	4.1	1.3		2.1	1.7			2.0
P3	E_B/eV	706.2	709.2	713.7	52.8	53.6	55.6	weak	178.4	160.5	160.8	162.0	—	399.8
	FWHM	0.8	3.9	8.6	1.8	2.4	4.4			3.0	1.3	1.3		1.6
P4	E_B/eV	706.3	709.4	713.7	53.2	54.1	56.8	—	—	—	161.2	162.8	—	399.8
	FWHM	1.1	3.9	6.4	1.5	3.2	4.0				1.2	1.3		1.9
P5	E_B/eV	706.4	709.4	713.9	52.3	54.1	56.6	—	—	—	161.0	162.2	—	399.8
	FWHM	1.4	4.1	7.2	1.7	2.6	3.0				1.1	1.2		1.9
P7	E_B/eV	706.4	709.7	715.1	52.4	54.0	56.8	—	—	—	161.4	163.0	—	399.9
	FWHM	0.9	4.6	5.7	1.5	2.9	3.1				1.0	1.1		1.8
P10	E_B/eV	706.5	708.6	712.7	52.1	53.5	56.2	—	—	—	161.4	162.9	164.2	399.9
	FWHM	1.00	4.1	7.7	1.3	2.8	4.7				1.0	0.8	0.8	1.7
Ave.	E_B/eV	706.4±0.2	709.3±0.4	713.9±0.7	52.6±0.4	54.0±0.4	56.3±0.4	53.3	178.5	160.4	161.2±0.3	162.6±0.4	164.2	399.8±0.1
	FWHM	1.00±0.2	4.1±0.3	7.4±1.1	1.4±0.3	2.7±0.3	3.9±0.6	1.3	—	—	1.2±0.3	1.1±0.2	0.8	1.8±0.1

P1, 0–4.0 cm; P2, 4.0–7.8 cm; P3, 7.8–11.6 cm; P4, 11.6–15.4 cm; P5, 15.4–19.2 cm; P6, 19.2–23.0 cm; P7, 23.0–26.8 cm; P8, 26.8–30.6 cm; P9, 30.6–34.4 cm; P10, 34.4–38.2 cm; P11, 38.2–40.0 cm.

corrections were made using the Shirley method (Shirley, 1972) for the Se 3d, Se $L_3L_{45}L_{45}$, S 2p, Ca 2p, N 1s, Si 2s, C 1s, and O 1s orbitals and by the Shirley-Tougaard method for the Fe 2p orbital. Peak shapes were defined using a Gaussian-Lorentzian function. The C–C bond has a well-defined position at E_B[C 1s] = 284.6 eV, which was used as a reference peak to correct for charging effects. XP-spectra were collected in the same manner for the reference materials: Se powder (99.999%, –100 mesh, Aldrich, 22986-5), ZnSe powder (99.99%, 5 μm, Aldrich, 24461-9), Fe-foil (99.99%, ALFA), ZVI, and ZVI washed with methanol. The XPS measurement is the most surface-sensitive of the techniques used, with escape depths of ≤25 Å.

Raman spectroscopy

Raman spectra were obtained with a Renishaw 1000 Raman microscope system. Excitation was accomplished by light of a single wavelength (514.5 nm) from Ar ion laser. The incident power was about 38 mW at the sample point. It is possible to distinguish between selenide and metallic selenium by Raman spectroscopy, because selenide has a Raman shift at 250.8 cm^{-1} whereas metallic selenium has a Raman shift at 232.8 cm^{-1}. Raman spectroscopy has a penetration range of 100 μm in depth and 5 μm in diameter, which is very coarse compared with the other techniques.

Electron spectroscopy

Scanning electron microscopy (SEM) and energy dispersive X-ray analysis (EDAX) were performed to obtain the information on the morphology and the composition of Se-bearing phases using a LEO 1530 SEM-EDAX operating at 20 kV. SEM-EDAX usually has analytical volumes of several cubic microns that are 2–3 μm in depth and diameter.

RESULTS AND DISCUSSION

XPS spectral data from the column specimens (P2~P10) and the reference materials are summarized in Tables 2 and 3. The peak binding energies (E_B) for Fe, Se, and S compounds, including ZVI and ZVI washed with methanol indicate that there is a strong overlap between the Se 3d and the Fe 3p binding energy ranges, and between the Se 3p and the S 2p binding energy ranges in Table 3.

The Se $L_3M_{45}M_{45}$ Auger spectra measured for the column samples P2, P3, P4, P5, P7 and P10 are shown in Fig. 2. There is no spectral interference from other elements found in these samples. The spectra show that Se species are most abundant in the P2 sample. The P3 sample has a trace amount of Se species. Samples P4~P10 have very little Se.
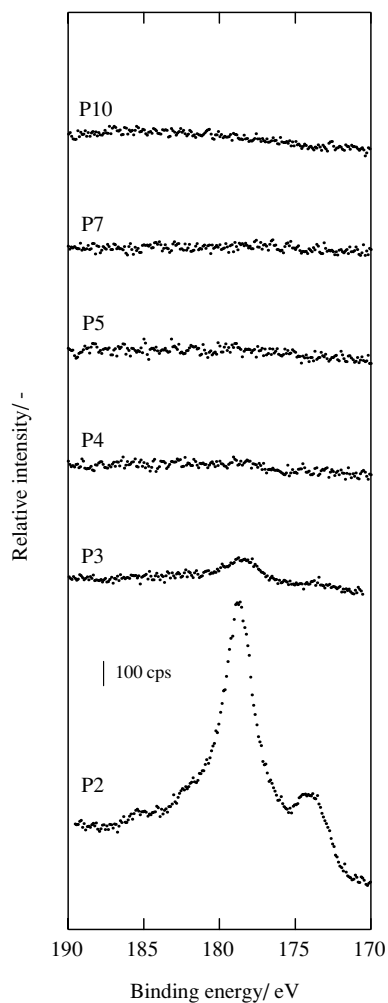
Fig. 2. XP-spectra of Se $L_3M_{45}M_{45}$ region for column contents after water treatment for 1200 h. Binding energy was corrected by $E_B[C1s_A]$ from hydrocarbon = 286.4 eV. A vertical bar indicates 50 cps.
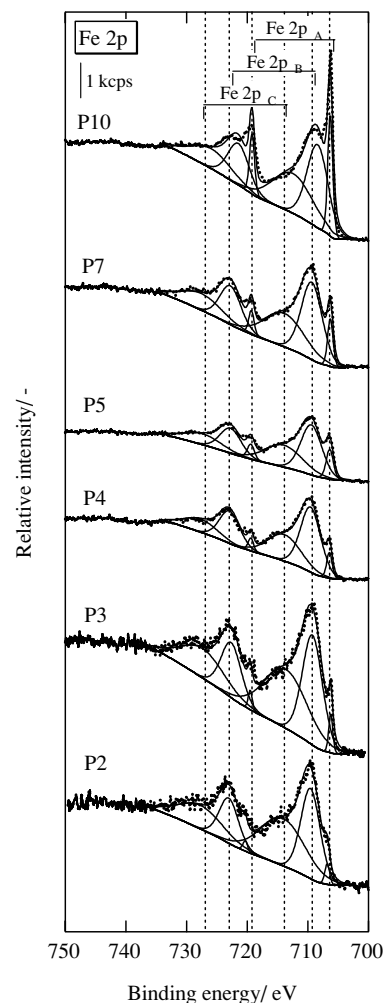
Fig. 3. XP-spectra of Fe 2p region for column contents after water treatment for 1200 h. Binding energy was corrected by $E_B[C1s_A]$ from hydrocarbon = 286.4 eV. A vertical bar indicates 1 kcps.

The measured XP spectra (dots) and the peak separation (lines) for Fe 2p for the column materials are shown in Fig. 3. Each spectrum was separated into three pairs of peaks: the first doublet (A) is assigned to metallic iron at $E_B[Fe\ 2p_{3/2}] = 706.4 \pm 0.2$ eV, the second doublet (B) is assigned to ferrous compounds at $E_B[Fe\ 2p_{3/2}] = 709.3 \pm 0.3$ eV, and the third doublet (C) is the residual, assigned to mainly ferric compounds at $E_B[Fe\ 2p_{3/2}] = 713.8 \pm 0.7$ eV. The peaks E_B and full width at half maximum (FWHM) are listed in Table 2. The first component is mainly from the fresh metallic iron precipitates formed by reduction of Fe(III) species at the corroded surface of ZVI, while the original ZVI has two species included in the second and third components (Table 2). Iron sulfides, which are produced by microbial reduction of sulfate, are included within the first component (Table 2). It is im-

possible, however, to distinguish between metallic iron and iron sulfides by $E_B[Fe\ 2p]$, because the spectra are very similar (Sasaki et al., 1993). There is a relatively minor abundance of the first component of Fe 2p in P2. It can be assumed that the principal electron acceptors are Se(VI) and SO_4. Very little metallic Fe is detected in the P2 sample.

The area ratio of components 1, 2 and 3 from each of the Fe 2p spectra should give the same results as components 1, 2 and 3 from each of the Fe 3p spectra. The Fe 3p peaks overlap with Se 3d range for all of the column samples, and the Se 3p peak overlaps with the S 2p region for P2 and P3 samples.

Figure 4 shows the measured XP spectra of the Se 3d-Fe 3p region for the column samples. The shape of the spectrum (dots) for P2 is quite different from those for
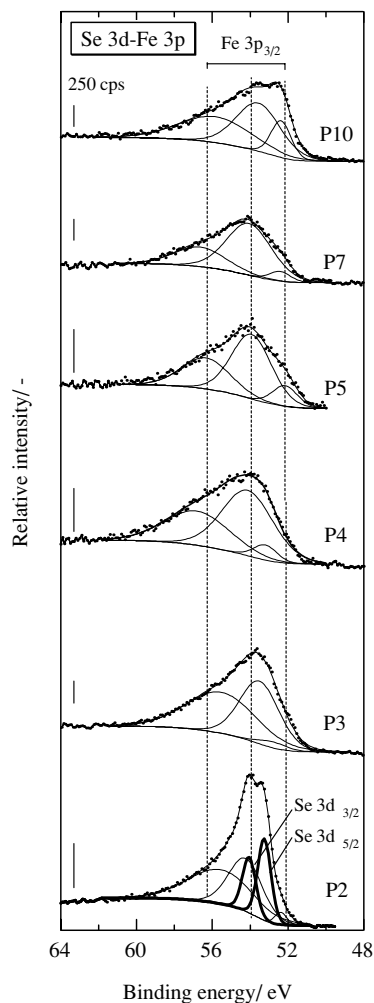
Fig. 4. XP-spectra of Se 3d-Fe 3p region for column contents after water treatment for 1200 h. Binding energy was corrected by $E_B[C1s_A]$ from hydrocarbon = 286.4 eV. Vertical bars indicate 250 cps.

Fig. 5. XP-spectra of S 2p-Se 3p region for column contents after water treatment for 1200 h. Binding energy was corrected by $E_B[C1s_A]$ from hydrocarbon = 286.4 eV. Vertical bars indicate 250 cps.

the other samples. The Fe $3p_{3/2}$, Se $3d_{3/2}$, and Se $3d_{5/2}$ peaks all contribute in this region of the spectra. Peak separation was performed assuming that there are three sets of Fe 3p peaks, for which the area ratio was calculated on the basis of the area ratio measured for the Fe 2p region (Fig. 3), and assuming that the residual represents a contribution from Se 3d. The area ratios for Se $L_3M_{45}M_{45}$, Se 3p, and Se 3d also were estimated based on the ratios of the standard substances ZnSe and metallic selenium. In Fig. 4, three iron species had E_B [Fe $3p_{3/2}$] = 52.6 ± 0.4, 54.0 ± 0.4, and 56.3 ± 0.4 eV. In addition, it was determined that the E_B [Se $3d_{5/2}$] was 53.3 eV for P2. This binding energy was not assigned to metallic selenium but to selenide (Table 3), though it is difficult to determine whether it corresponds to FeSe$_2$ or FeSe. Based on the above assumptions, the contribution of Se
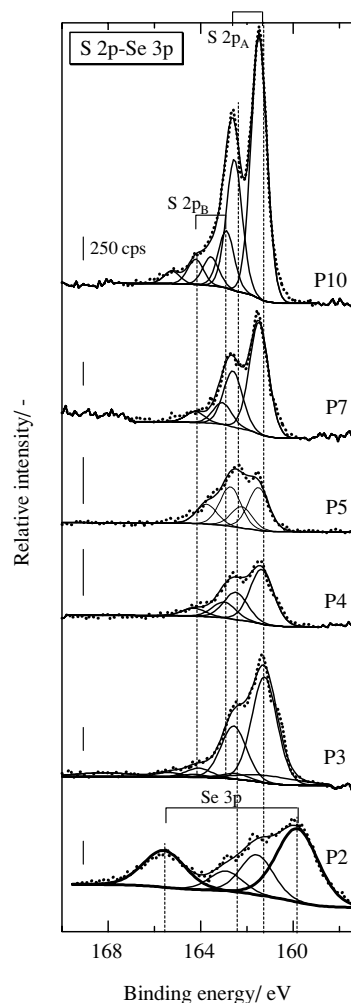
to this region was negligible in P3.

The XP spectra in the S 2p-Se 3p region for the column samples are shown in Fig. 5. Only the spectrum for sample P2 showed strong intensities around 160.2 eV and 165.8 eV of E_B. The spectrum was fit assuming that Se species are present only in the P2 sample, and that there are at least two kinds of sulfur species; sulfide and elemental sulfur in all spectra. The P2 sample spectra included two principal species, which are the Se $3p_{3/2}$ peak at E_B [Se $2p_{3/2}$] = 160 eV assigned to selenide, and the S $2p_{3/2}$ peak at E_B[S $2p_{3/2}$] = 161.5 eV assigned to sulfide. All the other spectra showed the peaks of two sulfur species, dominantly sulfide at E_B[S $2p_{3/2}$] = 161.5 eV and secondarily elemental sulfur at E_B[S $2p_{3/2}$] = 163.0 eV. It should also be noted that the P10 sample has an extremely large amount of sulfide at E_B [S $2p_{3/2}$] = 160.2 eV, el-
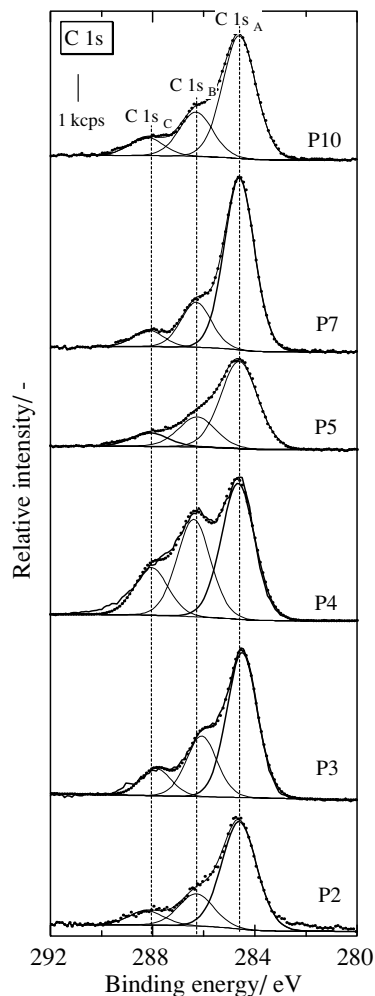
Fig. 6. XP-spectra of C 1s region for column contents after water treatment for 1200 h. Binding energy was corrected by $E_B[C1s_A]$ from hydrocarbon = 286.4 eV. A vertical bar indicates 1 kcps.

Fig. 7. XP-spectra of N 1s region for column contents after water treatment for 1200 h. Binding energy was corrected by $E_B[C1s_A]$ from hydrocarbon = 286.4 eV. A vertical bar indicates 250 cps.

emental sulfur at $E_B[S\ 2p_{3/2}] = 163$ eV, and a trace amount of an oxide form of sulfur at $E_B[S\ 2p_{3/2}] = 164.2$ eV, which might indicate incomplete sulfate reduction in this section of the column.

The C 1s spectrum was separated into three components (Fig. 6): the first one (A) is assigned to long chains of hydrocarbons, from air, pump oil vapor, reactants with water and the tape holding the powder, at $E_B[C\ 1s] = 284.6$ eV, the second one (B) is assigned to alcohol compounds at $E_B[C\ 1s] = 286.3$ eV, and the third one (C) is assigned to carboxyl and ketone compounds at $E_B[C\ 1s] = 288.0$ eV (Herbert *et al.*, 1998). The hydrocarbon intensity was used to normalize the relative intensity of the other components.

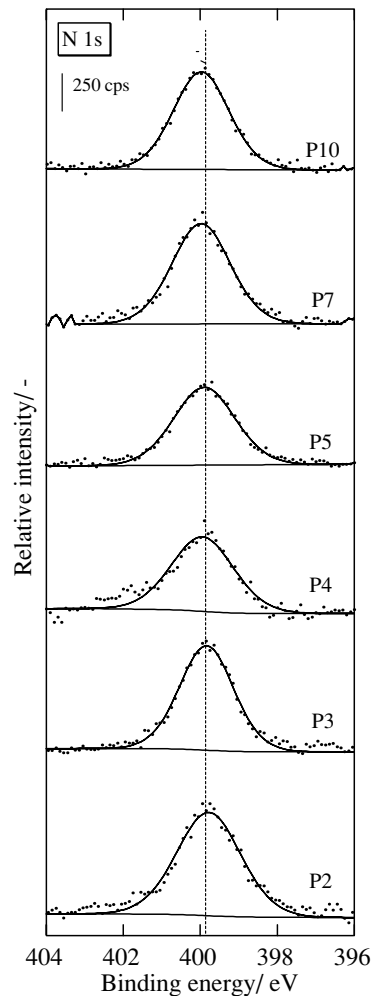Positions and relative intensities of Ca 2p, N 1s and Si 2s to the first C 1s peak were constant and independ-

ent of the column depth. The binding energy of Ca 2p, $E_B[Ca\ 2p_{3/2}]$, was 347.3 ± 0.16 eV, assigned to calcium carbonate. The column effluent is saturated with respect to calcite and dolomite according to MINTEQA2 calculations (Sasaki *et al.*, in press). The binding energy of N 1s, $E_B[N\ 1s]$, was 399.8 ± 0.07 eV (Fig. 7), which is assigned to amine compounds probably derived from the wood chips or saw dust, and is not likely a product microbiological reduction of nitrate and nitrite in the column because the biological denitrification produces N_2 not ammonium (Konhauser, 2007). The binding energy for Si 2s, $E_B[Si\ 2s]$, was 153.3 ± 0.08 eV, independent of the column depth, which is assigned to silicon oxides from very fine grains of silica sand and gravels. Sand and gravel were included in the column mixture as unreactive components.
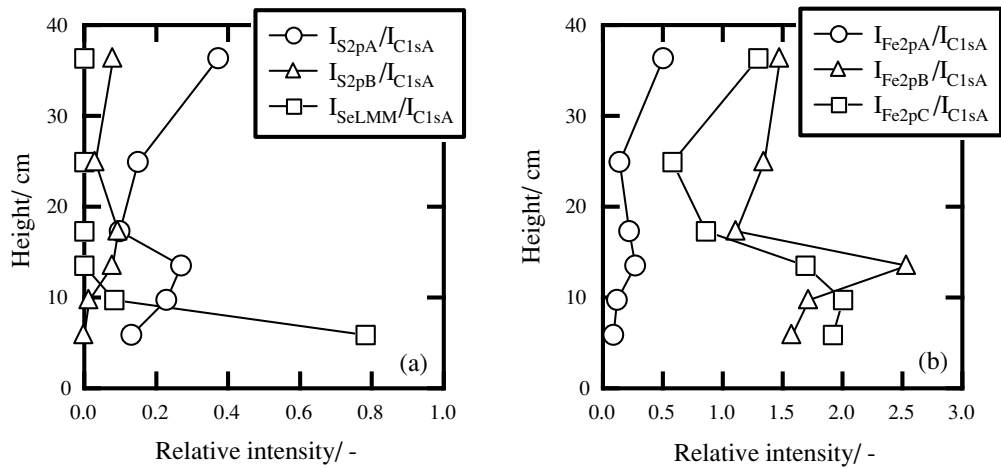
Fig. 8. Relative XPS derived area intensities of (a) $I_{[S\ 2pA]}/I_{[C1sA]}$, $I_{[S\ 2pB]}/I_{[C1sA]}$, $I_{[Se\ LMM]}/I_{[C1sA]}$, and (b) $I_{[Fe\ 2pA]}/I_{[C1sA]}$, $I_{[Fe\ 2pB]}/I_{[C1sA]}$, $I_{[Fe\ 2pC]}/I_{[C1sA]}$. The intensities of S $2p_A$, and S $2p_B$ correspond to sulfide and elemental sulfur. The intensities of Fe $2p_A$, Fe $2p_B$ and Fe $2p_C$ correspond to metallic iron and iron sulfides, respectively.
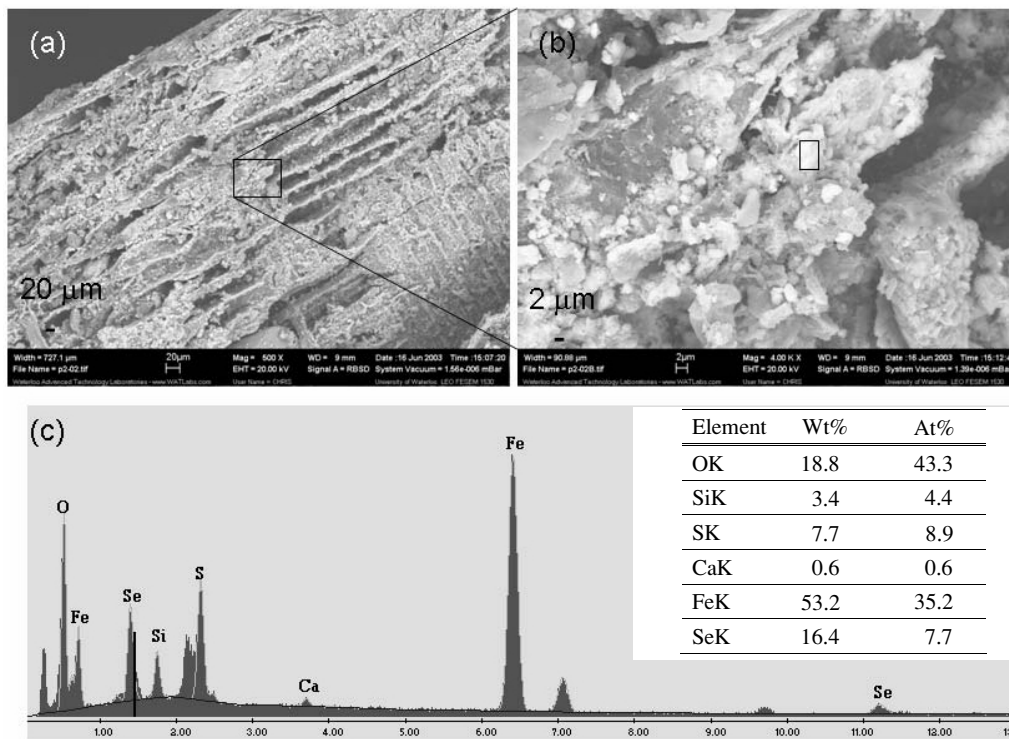

Element	Wt%	At%
OK	18.8	43.3
SiK	3.4	4.4
SK	7.7	8.9
CaK	0.6	0.6
FeK	53.2	35.2
SeK	16.4	7.7

Fig. 9. SEM-EDAX on the surface of ZVI particles of aquifer solids from P2 sample after 1200 hours. (a) Low magnification, (b) high magnification of the box in (a), and (c) elemental analysis within the box shown in (b).

Using the intensity of C $1s_A$, the relative intensities of iron, sulfur, and selenium species were also calculated as shown in Fig. 8. The Fe(II) species include uncorroded ZVI, and Fe(III) species, which are present as corrosion products on the ZVI grains. It is evident that selenide is more abundant in the P2 sample than in the other samples. In contrast, the abundances of metallic iron and iron sulfides increase toward the top of the column. Elemen-
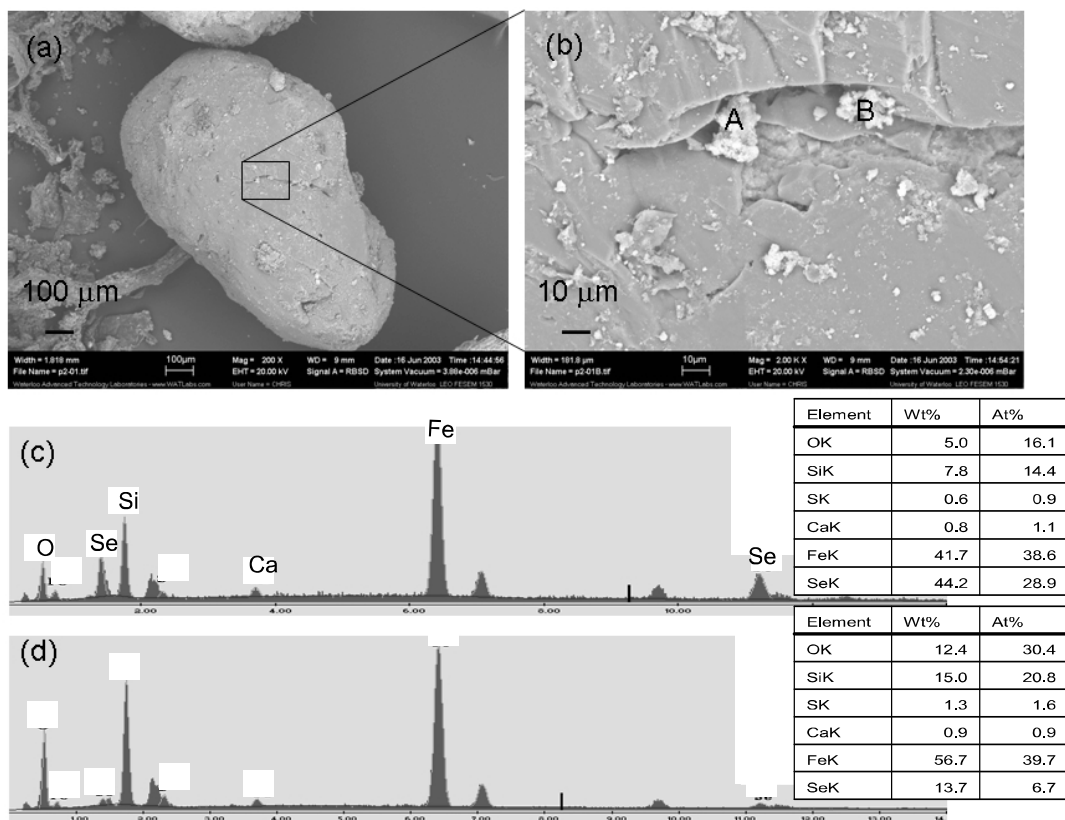
Fig. 10. SEM-EDAX of parts on the surface of silica sand particles from P2 sample after 1200 hours. (a) SEM image, (b) elemental spectra of A and B in (a), and (c) elemental compositions features A and B in (a).

Element	Wt%	At%
OK	5.0	16.1
SiK	7.8	14.4
SK	0.6	0.9
CaK	0.8	1.1
FeK	41.7	38.6
SeK	44.2	28.9

Element	Wt%	At%
OK	12.4	30.4
SiK	15.0	20.8
SK	1.3	1.6
CaK	0.9	0.9
FeK	56.7	39.7
SeK	13.7	6.7

tal sulfur is much less abundant than sulfide. More elemental sulfur was present in the P4~P10 samples than in the P2 and P3 samples.

Figure 9 shows SEM images and EDAX analyses of the surfaces of ZVI particles from sample P2. The morphology of the ZVI is very porous with many pits, resulting in a high surface area and potentially an abundance of reaction sites (Fig. 9(a)). Figure 9(b) shows an enlargement of framboidal particles, and a standardless semi-quantitative analysis for the selected area indicated ~8 atom% Se (Fig. 9(c)). These high Se concentration was detected on framboidal particles in the P2 sample. High Fe concentrations may be due to the presence of iron compounds other than iron sulfides and iron selenides. It is assumed that Se deposition on the surface of the ZVI was caused mainly by chemical reduction, because Se-reducing bacteria including *Sulfurodpirillum barnesiii*, *Euterobactor cloacae*, *Thauera selenatis*, *Enterobacter taylorae* and *Citerobacter frendii* have been reported to be capable of reducing Se(VI) to insoluble Se(0) (Cantafio *et al*., 1996; Losi and Frankenberger, 1997; Oremland *et al*., 1999; Zahir *et al*., 2003; Zhang *et al*., 2004). A few

framboidal particles containing large amounts of Se were also observed in the P3 sample materials. However, the overall Se content was much lower in the P3 sample than in the P2 sample.

Figure 10 shows an SEM image and EDAX analysis of two clusters of fresh precipitates on the surface of a silica sand particle from the P2 sample. Two points were analyzed by EDAX. Although the two morphologies are similar, the selenium contents were quite different. Cluster A has a Se/Fe atomic ratio of 0.8 whereas cluster B has a Se/Fe atomic ratio of 0.2. This observation suggests that Se is not always stoichiometrically involved in fresh iron precipitates but partly associated with fresh iron precipitates in the P2 sample. Elemental mapping of a thin section reveals that the high concentration of Se is present as needle-shaped particles which are up to a few micrometers in length. These needles are most likely elemental selenium (Fig. 11). Besides the elemental Se particles, Se is predominantly associated with Fe, indicating that Se in the P2 sample is deposited mostly in association with iron, and partly as elemental selenium. The ZVI removes oxygen in the column according to the reaction of
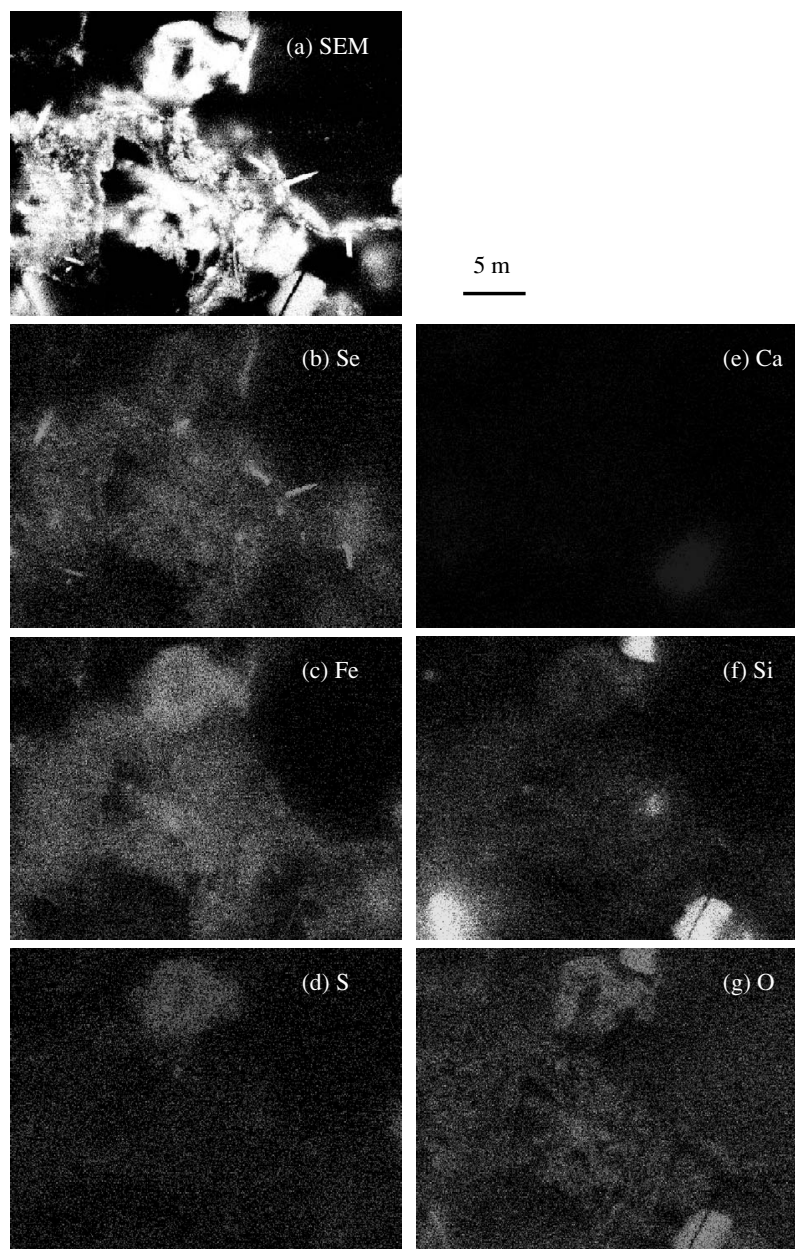
Fig. 11. Thin section SEM images and elemental mapping of Se, S, Fe, O, Si and Ca in aquifer solids from P2 samples after 1200 hours.

$2Fe(0) + 2H_2O + O_2 = 2Fe^{2+} + 4OH^-$, and serves electron donors by releasing hydrogen in the reaction of $Fe(0) + 2H_2O = Fe^{2+} + 2OH^- + H_2$, resulting in reduction of selenate to selenide and in stimulation of anaerobic microorganisms including sulfate-reducing bacteria and selenate-reducing bacteria. The magnitude of the microbiological contribution to the precipitation of elemental selenium might be clarified by determination of the selenium isotopic ratios.

Different from the P2 and P3 samples, precipitates in the P4, P7 and P10 samples are fibrous particles with no Se detected (Fig. 12). The P4 sample contains mainly iron sulfides with iron oxides as a secondary precipitate.

The P2 sample also was examined by Raman spectroscopy to provide another indication of selenium speciation. Figure 13 shows the Raman spectra for the P2 sample and the reference compounds. There is an observed broad Raman band which has the maximum at 253.2 cm^{-1} and shoulder peaks in the lower than the maximum position in the P2 spectrum (Fig. 13(a)), which may indi-
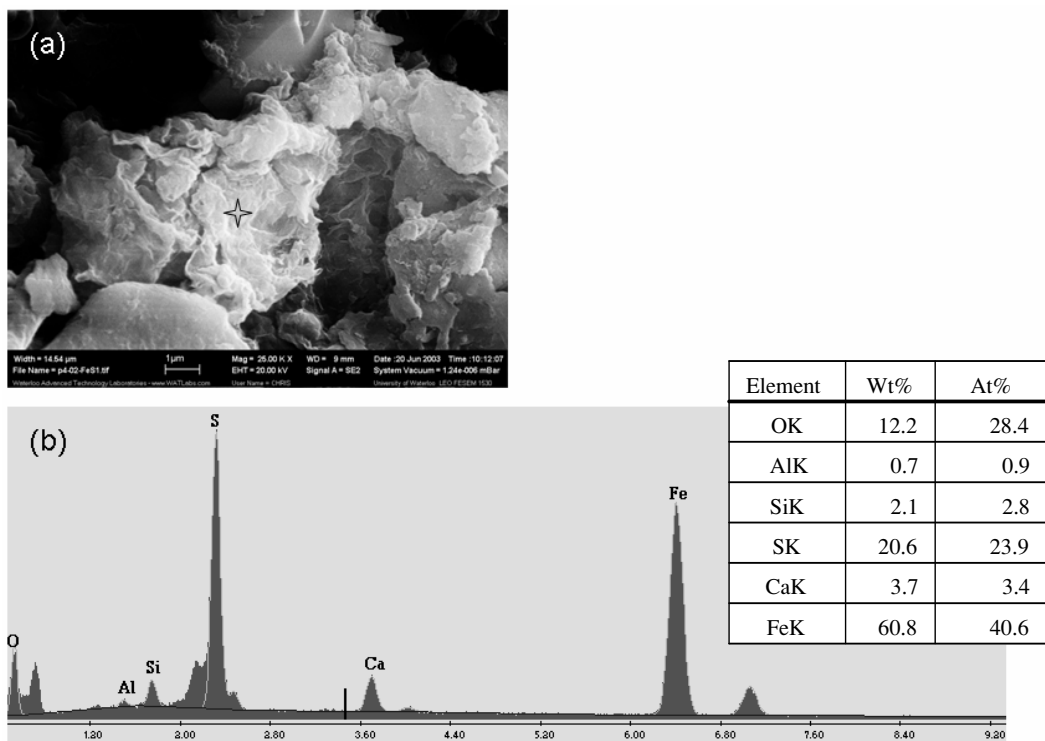
Fig. 12. SEM-EDAX on the surface of a fibrous particle on aquifer solids from P4 sample after 1200 hours. (a) SEM image and (b) elemental analysis of a star in (a).

Element	Wt%	At%
OK	12.2	28.4
AlK	0.7	0.9
SiK	2.1	2.8
SK	20.6	23.9
CaK	3.7	3.4
FeK	60.8	40.6

cate that P2 sample contains selenide with minor metallic selenium. The observation of a greater abundance of selenide appears to be consistent with the XPS results for selenium speciation. However, metallic selenium was not detected by XPS, probably because the XPS measurement is the most surface-sensitive of the techniques used, with escape depths of ≤25 Å.

An integrated interpretation of the results from the XPS, SEM-EDX, and Raman spectroscopy studies suggest that Se is precipitated as an iron selenide like ferroselite on the surface of ZVI, and a very minor amount as elemental selenium inside the framboidal particles. Additionally it was confirmed that the surface of ZVI granules was still in reactive phases of sulfides and Fe(0) over the Se-accumulated zone. The longevity of the present PRB column was estimated to be more than 75 years, assuming that the contaminated groundwater plume having 2 mg dm^{-3} selenate as Se at an average of linear velocity of 20 m per year is treated using the PRB, based on the efficiency and capacity of ZVI for Se removal, as well as sustenance of permeability (Sasaki *et al.*, in press). The present observations further provided the direct assurance that the surface of ZVI in upper zone is not covered with less reactive and less soluble Fe(III)-bearing minerals but still reactive. The PRBs are known as "passive" treatment of the contaminated groundwaters. The
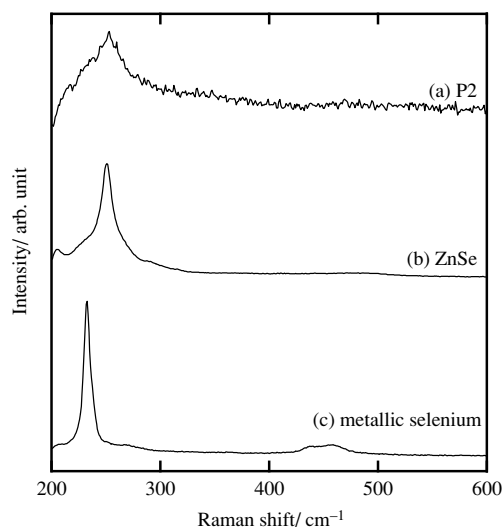

Fig. 13. Raman spectra of (a) the P2 sample, (b) ZnSe, and (c) metallic selenium.

present PRB designed with concept of chemical and biological remediation shows that selenate would be returned to the originally mineralogical phases like ferroselite and elemental selenium.

REFERENCES

Bahl, M. K. (1975) Relaxation during photoelectron and LMM Auger decay in arsenic and some of its compounds. *J. Chem. Phys.* **64**(3), 1210–1218.

Blowes, D. W., Ptacek, C. J., Benner, S. G., McRae, C. W. T., Bennett, T. A. and Puls, R. W. (2000) Treatment of inorganic contaminants using permeable reactive barriers. *J. Contam. Hydrol.* **45**, 123–137.

Cahen, D., Ireland, P. J., Kazmerski, L. L. and Thiel, F. A. (1985) X-ray photoelectron and Auger spectroscopic analysis of surface treatment and electrochemical decomposition of $CuInSe_2$ photoelectrodes. *J. Appl. Phys.* **57**(10), 4761–4771.

Canava, B., Vigneron, J., Etcheberry, A., Guillemoles, J. F. and Lincot, D. (2002) High resolution XPS studies of Se chemistry of a Cu(In, Ga)Se_2 surface. *Appl. Sur. Sci.* **202**, 8–14.

Cantafio, A. W., Hagen, K. D., Lewis, G. E., Bledsoe, T. L., Nunan, K. M. and Macy, J. M. (1996) Pilot-scale selenium bioremediation of San Joaquin drainage water with *Thauera selenatis*. *Appl. Environ. Microbiol.* **62**, 3298–3303.

Fishbein, L. (1991) *Metals and Their Compounds in the Environment: Occurrence, Analysis, and Biological Relevance* (Merian, E., ed.), 1153–1190, VCH, Weinheim.

Frankenberg, W. T. and Benson, S. (1994) *Selenium in the Environment*. Marcel Dekker, Inc., 456 pp.

Hamdadou, N., Bernede, J. C. and Khelil, A. (2002) Preparation of iron selenide films by selenization technique. *J. Crystal Growth* **241**, 313–319.

Herbert, R. B., Benner, S. G., Pratt, A. R. and Blowes, D. W. (1998) Surface chemistry and morphology of poorly crystalline iron sulfides precipitated in media containing sulfate-reducing bacteria. *Chem. Geol.* **144**, 87–97.

Islam, R. and Rao, D. R. (1996) X-ray photoelectron spectroscopy of $Zn_{1-x}Cd_xSe$ thin films. *J. Electron Spectrosc.* **81**, 69–77.

Iwakuro, H., Tatsuyama, C. and Ichimura, S. (1982) XPS and AES studies on the oxidation of layered semiconductor GaSe. *Jpn. J. Appl. Phys.* **21**(1), 94–99.

Konhauser, K. (2007) *Introduction to Geochemistry*. Blackwell Publishing, MA, U.S.A., pp. 266–268.

Konno, H. and Nagayama, M. (1980) X-ray photoelectron spectra of hexavalent iron. *J. Electron Spectrosc. Relat. Phenom.* **18**, 341–343.

Konno, H., Sasaki, K., Tsunkawa, M., Takamori, T. and Fruichi, R. (1991) X-ray photoelectron spectroscopic analysis of surface products on pyrite formed by bacterial leaching. *Bunseki Kagaku* **40**, 609–616.

Losi, M. E. and Frankenberger, W. T., Jr. (1997) Reduction of selenium oxyanions by Enterobacter cloacae strain SLDaa-1: Isolation and growth of the bacterium and its expulsion of selenium particles. *Appl. Environ. Microbiol.* **63**, 3079–3084.

Myneni, S. C. B., Tokunaga, T. K. and Brown, G. E., Jr. (1997) Abiotic selenium redox transformations in the presence of Fe(II, III) oxides. *Science* **278**, 1106–1109.

Oremland, R. S., Blum, J. S., BindiI, A. B., Dowdle, P. R., Herbel, M. and Stolz, J. F. (1999) Simultaneous reduction of nitrate and selenate by cell suspensions of selenium-respirating bacteria. *Appl. Environ. Microbiol.* **65**, 4385–4392.

Presser, T. S. and Swan, W. C. (1990) Geochemical evidence for Se mobilization by the weathering of pyretic shale, San Joaquin Valley, California, U.S.A. *Appl. Geochem.* **5**, 703–717.

Sasaki, K., Tsunekawa, M., Konno, H., Hirajima, T. and Takamori, T. (1993) Leaching behaviour and surface characterization of pyrite in bacterial leaching with *Thiobacillus ferrooxidans*. *J. Min. Mat. Proc. Inst. Jpn.* **109**, 29–35.

Sasaki, K., Blowes, D. W. and Ptacek, C. J. (in press) Immobilization of Se(VI) in mine drainage by permeable reactive barriers: column performance. *Appl. Geochem.*

Scherer, M. M., Richer, S., Valentine, R. L. and Alvarez, P. J. J. (2000) Chemistry and microbiology of permeable reactive barriers for in situ groundwater clean up. *Critical Reviews in Environmental Science and Technology* **30**, 363–411.

Shirley, D. A. (1972) High-resolution X-ray photoelectron spectrum of the valence bands of gold. *Phys. Rev.* **B5**, 4709–4714.

Stolz, J. F. and Oremland, R. S. (1999) Bacterial respiration of arsenic and selenium. *FEMS Microbiology Reviews* **23**, 615–627.

Ueno, T. and Odajima, A. (1982) X-ray photoelectron spectroscopy of Ag- and Cu-doped amorphous As_2Se_3 and $GeSe_2$. *Jpn. J. Appl. Phys.* **21**(2), 230–234.

Wagner, C. D. (1990) Photoelectron and Auger energies and the Auger parameter: A data set. *Practical Surface Analysis* (2nd ed.), (Beiggs, D. and Seah, M. P., eds.), John Wiley & Sons, Ltd., NJ.

Zahir, A. Z., Zhang, Y. Q. and Frankenberger, W. T., Jr. (2003) Fate of selenate metabolized by Enterobacter taylorae. *J. Agric. Food Chem.* **51**, 3609–3613.

Zhang, Y., Siddique, T., Wang, J. and Frankenberger, W. T., Jr. (2004) Selenate reduction in water by *Citerobacter freundii* isolated from a selenium-contaminated sediment. *J. Agric. Food Chem.* **52**, 1594–1600.

Zhang, Y., Wang, J., Amrheim, C. and Frankenberger, W. T., Jr. (2005) Removal of selenium from water by zero valence iron. *J. Environ. Quality* **34**, 487–495.